Nucleic Acids Research, 2005, Vol. 33, No. 10 ***3339–3350***
doi:10.1093/nar/gki642

Effect on DNA relaxation of the single Thr718Ala mutation in human topoisomerase I: a functional and molecular dynamics study

Giovanni Chillemi[1], Paola Fiorani[2], Silvia Castelli[2], Alessandro Bruselles[1,2], Piero Benedetti[3] and Alessandro Desideri[2,*]

[1]CASPUR Interuniversities Consortium for Supercomputing Applications, Via dei Tizii 6b, Rome 00185, Italy, [2]Department of Biology, National Institute for the Physics of Matter, University of Rome Tor Vergata, Via Della Ricerca Scientifica, Rome 00133, Italy and [3]Department of Biology, University of Padua, Via Ugo Bassi 58/B, Padua 35131, Italy

Received February 15, 2005; Revised and Accepted May 20, 2005

ABSTRACT

The functional and dynamical properties of the human topoisomerase I Thr718Ala mutant have been compared to that of the wild-type enzyme using functional assays and molecular dynamics (MD) simulations. At physiological ionic strength, the cleavage and religation rates, evaluated on oligonucleotides containing the preferred topoisomerase I DNA sequence, are almost identical for the wild-type and the mutated enzymes, as is the cleavage/religation equilibrium. On the other hand, the Thr718Ala mutant shows a decreased efficiency in a DNA plasmid relaxation assay. The MD simulation, carried out on the enzyme complexed with its preferred DNA substrate, indicates that the mutant has a different dynamic behavior compared to the wild-type enzyme. Interestingly, no changes are observed in the proximity of the mutation site, whilst a different flexibility is detected in regions contacting the DNA scissile strand, such as the linker and the V-shaped α helices. Taken together, the functional and simulation results indicate a direct communication between the mutation site and regions located relatively far away, such as the linker domain, that with their altered flexibility confer a reduced DNA relaxation efficiency. These results provide evidence that the comprehension of the topoisomerase I dynamical properties are an important element in the understanding of its complex catalytic cycle.

INTRODUCTION

Eukaryotic topoisomerase I (Top1) is a monomeric enzyme that catalyzes the relaxation of supercoiled DNA during important processes including DNA replication, transcription, recombination and chromosome condensation (1–3). Human topoisomerase I (hTop1) is composed of 765 aminoacids, and the crystal structure of the N-terminal truncated protein (topo70) together with proteolytic experiments have shown that the enzyme is composed of four different domains: N-terminal domain (residues 1–214), core domain (residues 215–635), linker domain (residues 636–712) and C-terminal domain (residues 713–765) (4–6).

The catalytic cycle of the enzyme involves a nucleophilic attack of the active site tyrosine (Tyr-723) on the DNA backbone resulting in a breakage of one DNA strand, with the enzyme covalently attached to the 3′-phosphate at the nick. According to the 'rotation model', the enzyme changes the linking number of DNA allowing the free 5′-DNA substrate to rotate around the intact strand. It has been proposed that this rotation could be partially controlled by the linker domain and the V-shaped α helices (α6 from core subdomain I and α5 from core subdomain II, Figure 1). A second nucleophilic attack, driven now by the 5′-hydroxyl DNA end, restores intact DNA and frees enzyme (6).

Human topoisomerase I is of significant medical interest being the only target of the antitumor drug camptothecin (CPT). CPT reversibly binds to the covalent intermediate DNA–enzyme, stabilizing the cleavable complex and reducing the rate of religation. The stalled topoisomerase I collides with the progression of the replication fork producing lethal double-strand DNA breaks and cell death (1,7). Recently, an

*To whom correspondence should be addressed. Tel: +39 06 72594376; Fax: +39 06 2022798; Email: desideri@uniroma2.it

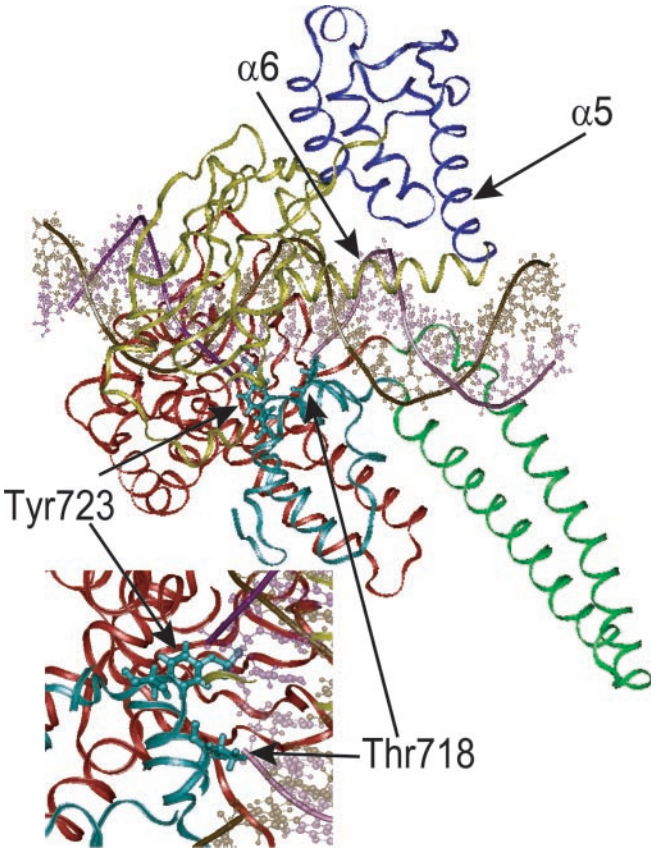

Figure 1. Topo70 hTop1 structure in complex with duplex DNA. Core Subdomains I, II and III are rendered in yellow, blue and red, respectively. Linker and C-terminal domains are rendered in green and cyan, respectively. The region containing the catalytic Tyr-723 and the mutated Thr-718 is highlighted in the insert.

important contribution toward the understanding of the interaction of CPT with topoisomerase I and DNA has been provided by the crystal 3D structure of the ternary complex between topo70 covalently linked to DNA and the CPT derivative Topotecan (8). The structure shows that the drug intercalates into the DNA duplex and moves the 5′-hydroxyl end of the DNA away from the scissile phosphate. This misalignment of the two ends probably slows down the religation step. Besides the effects on the religation reaction, CPT binding also reduces the linker domain mobility. This long-range effect has been highlighted by the fact that the linker shows a defined electron density in the structure of the Topotecan–DNA–topo70 ternary complex, but not in that of the DNA–topo70 binary complex (8). Moreover, the presence of the linker domain is required for a full CPT inhibition (9) and recently we have demonstrated that a single mutation in the linker domain confers CPT resistance (10). Finally, it has been also proposed that the drug effect is not limited to the slowing of the religation, but also includes the hindering of DNA rotation (11).

A CPT-like behavior has been proposed for the threonine 722 to alanine mutant, first isolated in yeast by Megonigal and coauthors (12). This mutant, when expressed in *Saccharomyces cerevisiae* exhibits a dramatic reduction in cell viability, enhancing the stability of the cleavable complex, with a mechanism similar to the action of CPT (12). The same mutation introduced in the corresponding residue 718 of the human enzyme (htop1Thr718Ala) shows a similar phenotype (13).

To gain further information on the CPT inhibition mechanism, we have compared wild-type and htop1Thr718Ala enzymes measuring the cleavage, relaxation and religation steps, while the intra and inter-domain communications have been analyzed through molecular dynamics (MD) simulation. The data indicate that the htop1Thr718Ala mutant slows down DNA relaxation, probably because of an altered dynamics at the level of the linker domain and the V-shaped α helices.

MATERIALS AND METHODS

Yeast strains and plasmids

ANTI-FLAG M2 affinity gel Freezer-Safer, FLAG peptide and M_2 monoclonal antibody were purchased from Sigma. *S.cerevisiae* strain EKY3 (*ura3-52*, *his3Δ200*, *leu2Δ1*, *trp1Δ63*, *top1*::*TRP1*, *MAT*α was described previously (14,15). Plasmid YCpGAL1-hTop1 in which the hTop1 is expressed under the galactose-inducible promoter in a single copy plasmid, has been described (15,16). htop1Thr718Ala was generated by oligonucleotide-directed mutagenesis of the hTop1 gene, and then cloned into BamHI–SalI-cut pBM126 to yield YCpGAL1-htop1Thr718Ala. The epitope-tagged construct YCpGAL1-heTOP1 contains the N-terminal sequence DYKDDDY recognized by the M_2 monoclonal antibody. The epitope-tag was subcloned into YCpGAL1-htop1Thr718Ala to produce YCpGAL1-hetop1Thr718Ala (13). The oligos used for the religation experiment were kindly provided by Mary-Ann Bjornsti, St Jude Children's Research Hospital, Memphis, TN.

Purification of DNA topoisomerase I

To purify heTOP1 and heTop1Thr718Ala EKY3, cells were transformed with YCpGAL1-heTOP1 and YCpGAL1-hetop1Thr718Ala, grown on SC-uracil plus 2% dextrose and diluted 1:100 in SC-uracil plus 2% raffinose. At an optical density of A_{595} = 1.0, the cells were induced with 2% galactose for 6 h. Cells were then harvested by centrifugation, washed with cold water and resuspended in 2 ml buffer/g cells using a buffer containing 50 mM Tris, pH 7.4, 1 mM EDTA, 1 mM ethylene glycol bis(β-aminoethyl ether)-*N*,*N*,*N*′,*N*′-tetraacetic acid, 10% (v/v) glycerol completed with protease inhibitors cocktail (Roche 1836153), and supplemented with 0.1 mg/ml sodium bisulfite and 0.8 mg/ml sodium fluoride. After addition of 0.5 vol of 425–600 μm diameter glass beads, the cells were disrupted by vortexing for 30 s alternating with 30 s on ice. The lysate were centrifuged and KCl 0.15 M final concentration was added to the sample prior to loading onto 2 ml ANTI-FLAG M2 affinity gel column equilibrated as described in the technical bulletin (Sigma). The column was washed with 20 column volumes of Tris-buffered saline (TBS) (50 mM Tris–HCl and 150 mM KCl, pH 7.4). Elution of FLAG-fusion-heTop1 was performed by competition with five column volumes of a solution containing 100 μg/ml FLAG peptide in TBS. Fractions of 500 μl were collected and glycerol 40% final concentration was added; all preparations were stored at −20°C. The fractions were resolved by SDS–PAGE; protein concentration and integrity were measured through immunoblot assay,

using the epitope-specific monoclonal antibody M_2. After normalization to the same amount of protein, the activity of the wild-type and mutant DNA topoisomerase I, as assayed by relaxation of supercoiled DNA at 150 mM KCl, has been found almost identical. In all the biochemical experiments, the same amount of wild-type and mutated protein has been used.

DNA Top1 activity *in vitro*

Top1 activity was assayed with a DNA relaxation assay (14–17). Top1 preparations were incubated in 30 µl reaction volume containing 0.5 µg (DNA excess) or 0.05 µg (enzyme excess) of negatively supercoiled plasmid pHC624 and reaction buffer (20 mM Tris–HCl, 0.1 mM Na_2EDTA, 10 mM $MgCl_2$, 50 µg/ml acetylated BSA and 150 mM KCl, pH 7.5). Reactions were stopped with a final concentration of 0.5% SDS after 1 h at 37°C. The supercoiled pHC624 DNA, that is present in both monomeric and dimeric forms, has been used as substrate. The presence of these two forms permits to follow the relaxation efficiency of the enzyme with two different substrates.

To assess the effects of ionic strength on enzyme activity, KCl was added in the DNA relaxation assay. The reaction was stopped with a final concentration of 0.5% SDS, and electrophoresis of the samples was carried out in a 1% agarose gel. DNA was visualized by staining of the gel with ethidium bromide and the gel image was analyzed using the ImageQuant software. The percentage of relaxation, measured as the amount of supercoiled plasmid converted to the relaxed form, is plotted as a function of salt concentration.

Kinetics of religation using oligonucleotide substrate

Oligonucleotide substrate CL14 (5′-GAAAAAAGACTTAG-3′) was radiolabeled with [γ-^{32}P]ATP at its 5′ end. The CP25 complementary strand (5′-TAAAAATTTTTCTAAGTCTTT-TTTC-3′) was phosphorylated at its 5′ end with unlabeled ATP. The two strands were annealed at a 2-fold molar excess of CP25 over CL14 as described (10). CL14/CP25 (20 nM) was incubated with an excess of enzyme for 60 min at 23°C followed by 30 min at 37°C in 20 mM Tris (pH 7.5), 0.1 mM Na_2EDTA, 10 mM $MgCl_2$, 50 µg/ml acetylated BSA and 150 mM KCl. Once cleavage had occurred, KCl was added to a final concentration of 0.5 M in order to inhibit further cleavage by the enzyme. Religation reactions were initiated by adding a 200-fold molar excess of R11 oligonucleotide (5′-AGAAAAATTTT-3′) over the duplex CL14/CP25. For various time points at 37°C, 5 µl aliquots were removed and the reaction was stopped with 0.5% SDS. After ethanol precipitation, samples were resuspended in 5 µl of 1 mg/ml trypsin and incubated at 37°C for 30 min. Samples were analyzed by denaturing urea/PAGE. The percentage of the remaining covalent complex (cleavage 1) was determined by PhosphorImager and ImageQuant software, and normalized on the total amount of radioactivity in each lane. The religation rate (k_r) was determined by fitting the data to the equation $\ln(\%\ \text{remaining cleavable complex}) = 4.605 - k_r t$ (9).

DNA religation was also assessed using alternative methods described by Colley *et al*. (18), which permits in a single experiment to detect both cleaved and religated oligonucleotides. Briefly, 20 nM CL14/CP25 was incubated with a 10-fold excess of the complementary R11 religation strand (5′-AGAAAAATTTT-3′) in 20 mM Tris–HCl, pH 7.5, 10 mM $MgCl_2$, 0.1 mM EDTA, 50 µg/ml acetylated BSA at 50 or 150 mM KCl. An identical concentration of native or mutated enzyme was added at 25°C. Aliquots (5 µl) were taken, as function of time, and the reaction was stopped adding 0.5% SDS and heating up to 75°C. Reaction products were resolved in 20% acrylamide/7 M urea gels and visualized with a PhosphorImager. This procedure permits to well separate the enzyme-bound cleaved oligonucleotide from the unbound religated oligonucleotide product.

Kinetics of cleavage using oligonucleotide substrate

The duplex (CL14/CP25) substrate was generated as described above. The suicide cleavage reactions were carried out by incubating 20 nM of the duplex with an excess of enzyme in 20 mM Tris (pH 7.5), 0.1 mM Na_2EDTA, 10 mM $MgCl_2$, 50 µg/ml acetylated BSA and 150 mM KCl at 23°C in a final volume of 50 µl as described by Yang and Champoux (19). A 5 µl sample of the reaction mixture before the addition of the protein was removed and used as the zero time point. At various time points, 5 µl aliquots were removed and the reaction stopped with 0.5% SDS. After ethanol precipitation, samples were resuspended in 5 µl of 1 mg/ml trypsin and incubated at 37°C for 30 min. Samples were analyzed by denaturing urea/PAGE. The percentage of cleavage 1 was determined by PhosphorImager and ImageQuant software and normalized on the total amount of radioactivity in each lane. The kinetics of cleavage was also followed through the enzyme-bound cleaved oligonucleotide product as described in the previous section.

Cleavage/religation equilibrium

Oligonucleotides CL25 (5′-GAAAAAAGACTTAGAAAAA-TTTTTA-3′) was radiolabeled with [γ-^{32}P]ATP at its 5′ end. The CP25 complementary strand (5′-TAAAAATTTTTCTA-AGTCTTTTTTC-3′) was phosphorylated at its 5′ end with unlabeled ATP. The two strands were annealed at a 2-fold molar excess of CP25 over CL25. Duplex CL25/CP25 (10 nM) was incubated with an excess of enzyme at 25°C in 20 mM Tris, pH 7.5, 0.1 mM Na_2EDTA, 10 mM $MgCl_2$, 50 µg/ml acetylated BSA and either 50 or 150 mM KCl. After 30 min, the reaction was stopped adding 0.5% SDS and either heating up to 75°C or precipitating with ethanol and digesting with trypsin. Reaction products were resolved in 20% acrylamide/7 M urea gels and the percentage of cleavage (%Cl) was determined using a PhosphorImager and ImageQuant software. The value of the cleavage/religation equilibrium constant (K_{cr}) has then been calculated from the equation $K_{cr} = \%\text{Cl}/(100 - \%\text{Cl})$.

MD simulations

The topo70–DNA covalent complex was modeled obtaining the starting position for residues 215–633 and 641–765 from the crystal structure 1a36 (6), and those for residues 203–214 from the crystal structure 1ej9 (5). The seven residues constituting the loop region that connects the linker to the core domain [residues 634–640, which are lacking in the 1a36 Protein Data Bank (PDB) structure because of thermal fluctuation] and the covalent bond between Tyr-723 and the DNA-1 base were added to the system by molecular modeling

using the SYBYL program (Tripos Inc., St Louis, MO). The same procedure has been followed to reconstruct the partially missing sidechains of the residues not fully detected in the X-ray diffraction structure. The spatial environment of each new residue was checked for close contact or overlap with neighboring residues, and stereochemical regularization of the structures was obtained by the Powell minimization method implemented in the SYBYL program. Residue 718 has been changed from threonine to alanine to generate the mutant topo70–DNA complex.

The systems were modeled with the AMBER95 all atom force-field (20), and placed in a rectangular box ($127 \times 84 \times 108$ Å^3) filled with TIP3P water molecules (21). Na^+ counterions were added to make the system electro neutral. The resulting total systems contained 9417 protein atoms, 1401 DNA atoms, 21 Na^+ counterions and 28 313 water molecules for topo70, giving a total of 95 778 atoms; and 9413 protein atoms, 1401 DNA atoms, 21 Na^+ counterions and 28 314 water molecules for the Thr718Ala mutant, giving a total of 95 777 atoms. All the system atoms have been subjected to an unconstrained simulation that allows the movement of both protein and DNA atoms. Note that this large number of atoms require efficient parallel computers to be simulated. Simulation of one of the two systems for 3250 ps required 408 h of wall clock time on eight CPUs of the IBM sp4 (Power4 at 1.3 GHz). The systems were simulated in periodic boundary conditions, using a cutoff radius of 9 Å for the non-bonded interactions, and updating the neighbor pair list every 10 steps. The electrostatic interactions were calculated with the Particle Mesh Ewald method (22,23). The SHAKE algorithm (24) was used to constrain all bond lengths involving hydrogen atoms. Optimization and relaxation of solvent and ions were initially performed keeping the solute atoms constrained to their initial position with decreasing force constants of 500, 25, 15 and 5 kcal/(mol Å). The systems have been simulated for 3250 ps at a constant temperature of 300 K using Berendsen's method (25) and at a constant pressure of one bar with a 2 fs time step. Pressure and temperature coupling constants were 0.5 ps. The analyses reported in this manuscript refer to the last 3000 ps of the trajectory (i.e. from 250 to 3250 ps), since the trend of the root mean square deviations (RMSDs) indicates that the systems are well stabilized after 250 ps.

The principal component analysis (26,27), the direct hydrogen bonds, the RMSDs and root mean square fluctuations (RMSF) have been calculated using the GROMACS MD package version 3.1.4 (28). The water-mediated hydrogen bond calculation has been carried out using an in-house written code, based on the GROMACS g_hbond code.

RESULTS

Relaxation activities of hTop1 and hTop1Thr718Ala

In order to analyze the different ionic strength requirement for the hTop1Thr718Ala and the wild-type protein, a relaxation plasmid assay was performed using a DNA substrate constituted by a dimeric (DSC) and monomeric (MSC) form (Figure 2A). The data plotted in Figure 2B indicate that, with both substrates, the two enzymes have their maximum relaxation efficiency in the 100–200 mM range whereas at low salt concentration (50 mM), the mutant is more efficient than the wild-type. The different salt profile shown by the wild-type and the mutated enzyme suggests a different electrostatic behavior. However, since the single mutation does not concern a charged residue, this effect is probably due to different structural–dynamical properties that modulate the interaction with DNA. At physiological salt concentration (150 mM KCl), the two enzymes show a maximum and comparable relaxation activity, therefore all the results presented in this paper have been carried out at this salt concentration.

The catalytic process of topoisomerase I is composed of different steps such as DNA association, cleavage, strand rotation, ligation and dissociation. In order to test the role played by the association and dissociation rates, the relaxation activities of the native and mutated enzyme have been assayed either with excess of supercoiled DNA relative to enzyme (in a time range from 0.5 to 60 min, Figure 3A), or with excess of enzyme compared to DNA (in a time range from 4 to 480 s, Figure 3B). In both experimental conditions, the native enzyme relaxes supercoiled DNA three to four times faster than the mutant. The absence of any effect of the enzyme/DNA ratio on the relaxation experiments indicates that the lower relaxation efficiency of the mutant cannot be ascribed to varied association/dissociation rates, but must be found in the cleavage/strand-rotation/religation steps of catalysis (29).

Cleavage and religation rate of hTop1 and hTop1Thr718Ala

In order to understand the cleavage religation property of the mutated enzyme, we have carried out a cleavage/religation equilibrium experiment on a 25mer full duplex oligonucleotide substrate CL25 (5′-GAAAAAGACTTAGAGAAAA-ATTTT-3′)/CP25 at medium (150 mM KCl) and low (50 mM KCl) ionic strength (Figure 4). At 150 mM KCl, the intensity of the band due to the cleavable complex is identical for both enzymes indicating that in this condition the enzymes are characterized by identical cleavage/religation equilibrium constant. In detail, evaluation of the cleavage percentage of the labeled scissile strand using the PhosphorImager and ImageQuant software indicates that K_{cr} is 2×10^{-4} for both enzymes.

On the other hand at 50 mM KCl, the equilibrium of the hTop1Thr718Ala is shifted toward the cleavable complex when compared to the wild-type enzyme. Quantitative evaluation of K_{cr} gives a value of 3×10^{-4} and 9×10^{-4} for the wild-type and the Thr718Ala mutant, respectively. A similar behavior has been observed at 50 mM KCl for a 900 bp DNA fragment where the Thr718Ala mutation shifted the equilibrium toward cleavage, as detected by the presence of several covalent enzyme–DNA intermediates (13).

Since the cleavage/religation equilibrium constant, for a linear DNA substrate can be defined as $K_{cr} = k_{cl}/k_r$, the experiment reported in Figure 4 suggests that at physiological ionic strength, the native and mutated enzymes are characterized by identical cleavage (k_{cl}) and religation (k_r) rates. In order to verify that the identical equilibrium constant is not due to an identical variation of the cleavage and religation rate, the cleavage chemical step has been investigated using a 5′ end radiolabeled suicide substrate CL14 (5′-GAAAAAAGACT-T$^{\downarrow}$AG-3′), containing the preferred Top1 sequence (marked

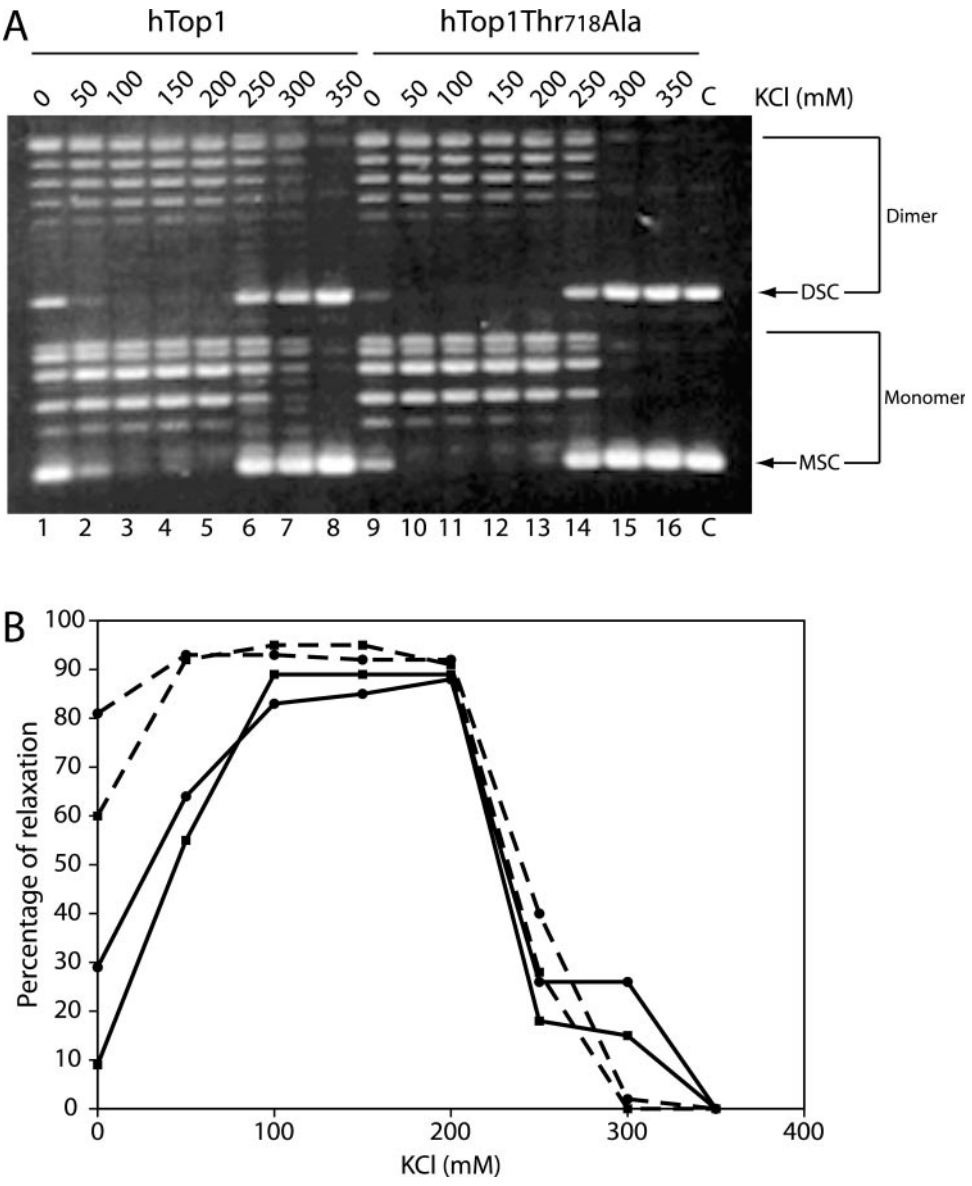

Figure 2. (**A**) Relaxation of negative supercoiled plasmid DNA of purified hTop1 (lanes 1–8) and hTop1Thr718Ala (lanes 9–16) at KCl concentrations of 0, 50, 100, 150, 200, 250, 300 and 350 mM. Reaction products were resolved in an agarose gel and visualized by ethidium bromide staining. The dimeric and monomeric forms of the supercoiled plasmid DNA are indicated by 'DSC' and 'MSC', respectively. Lane C, no protein added. (**B**) Percentage of relaxation measured as the amount of monomeric (squares) and dimeric (circles) supercoiled plasmid converted to the relaxed form by hTop1 (full line) and hTop1Thr718Ala (dotted line), plotted as a function of salt concentration.

by the arrow), annealed to the CP25 (5′-TAAAAATTTTTC-TAAGTCTTTTTTC-3′) complementary strand, to produce a duplex with an 11-base 5′ single-strand extension. With this substrate, the religation step is excluded because the short oligonucleotide (AG-3′) generated during cleavage cannot be religated, leaving the enzyme covalently attached to the 12 oligonucleotide 3′ end (9). The suicide cleavage substrate has been incubated with an excess of hTop1 or hTop1Thr718Ala in a time course experiment. The amount of cleaved fragment, normalized to the plateau value of the hTop1, has been plotted as a function of time in Figure 5A. Data show that both enzymes have an almost identical cleavage rate (k_{cl}), reaching in a comparable time a plateau that, however, has a lower value for the hTop1Thr718Ala mutant. Any quantitative evaluation of k_{cl} from the slope of the first part of the curve has been unsuccessful due to the paucity of experimental points present in this region.

DNA religation step has then been studied by testing the ability of both enzymes to religate the oligonucleotide R11 (5′-AGAAAAATTTT-3′) added to the cleaved suicide substrate. The first step of the assay consists in the incubation of an excess of hTop1 or hTop1Thr718Ala with the suicide substrate for 60 min in order to generate the cleaved complex with the enzyme covalently attached to the 3′ end. Once cleavage has occurred, the salt concentration is raised to 0.5 M KCl to prevent further cleavage activity by the enzyme (19) and the R11 oligonucleotide is then added to the mixture to initiate the ligation process. Aliquots have been removed at different

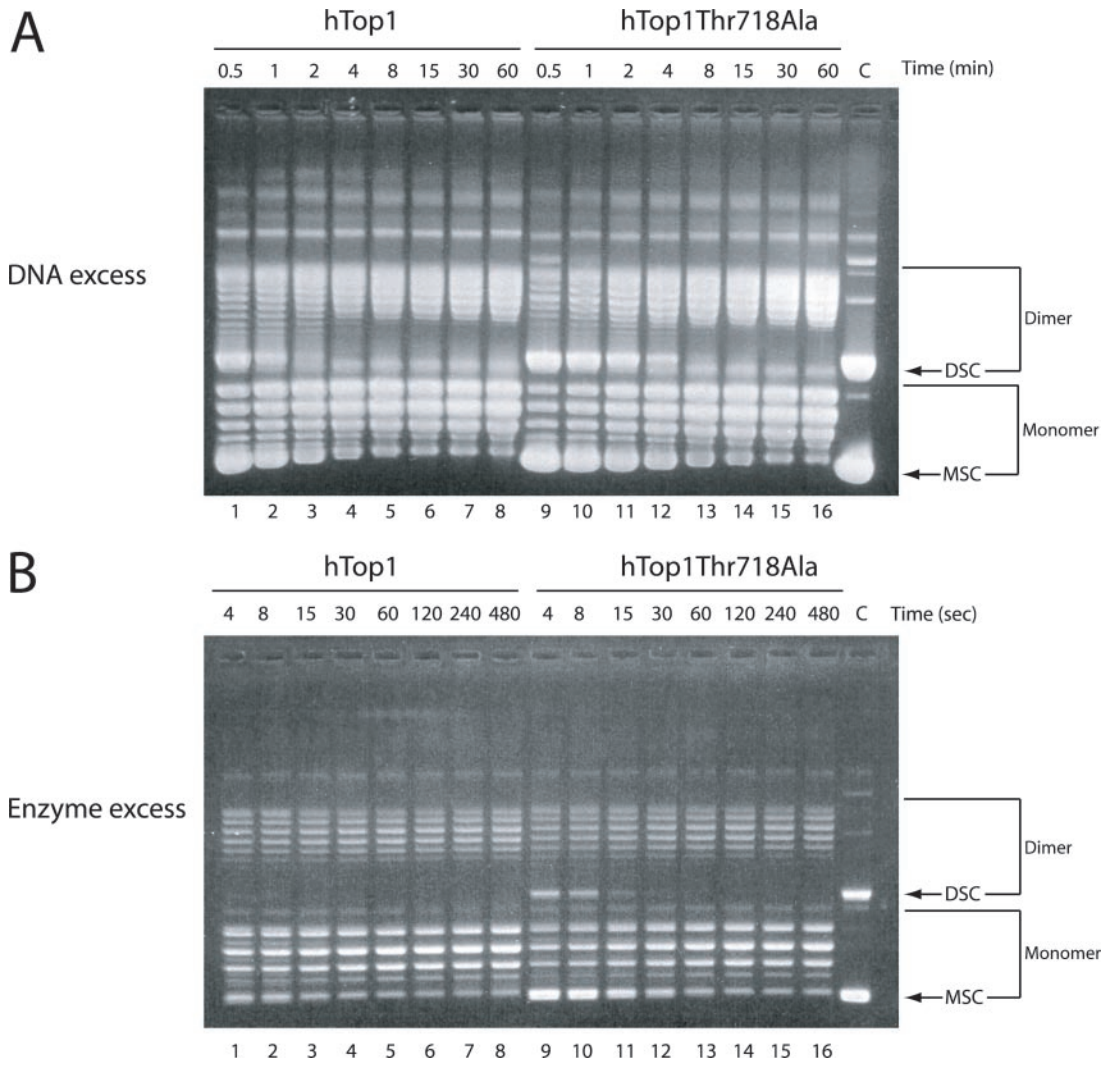

Figure 3. Relaxation kinetics for hTop1 and hTop1Thr718Ala at their salt optima concentrations. (**A**) Purified hTop1 (lanes 1–8) and hTop1Thr718Ala (lanes 9–16) were incubated with 0.5 μg/ml supercoiled plasmid DNA for 0.5, 1, 2, 4, 8, 15, 30 and 60 min at 37°C at 150 mM KCl. (**B**) Purified hTop1 (lanes 1–8) and hTop1Thr718Ala (lanes 9–16) were incubated with 0.05 μg/ml supercoiled plasmid DNA for 4, 8, 15, 30, 60, 120, 240, 480 s at 37°C at 150 mM KCl. The dimeric and monomeric forms of the supercoiled plasmid DNA are indicated by 'DSC' and 'MSC', respectively. Lane C, no protein added.

times, the reaction stopped by addition of SDS and the products analyzed by PAGE. The percentage of the remaining cleaved complex, determined as described under Materials and Methods, plotted as a function of time in Figure 5B indicates that hTop1 and hTop1Thr718Ala have very similar religation rates (k_r), their values, evaluated from the decay of the curve, being equal to 0.14 and 0.19 min^{-1}, respectively. The identity of the religation rate, k_r, and of the cleavage/religation equilibrium, K_{cr}, indicates that the chemistry of the enzyme at 150 mM KCl is identical for both the wild-type and the mutated enzyme and that these steps of the enzymatic reaction cannot be the origin of the reduced relaxation efficiency of the mutant.

The cleavage and religation efficiency of the wild-type and mutated enzyme has been also tested in a single experiment using the procedure described by Colley *et al*. (18) at two different ionic strengths, namely at 50 and 150 mM KCl. At 150 mM KCl, hTop1 and hTop1Thr718Ala display a similar behavior, in agreement with the previously described experiments (Figure 5) characterized by an almost equal cleavage and religation rate. On the other hand at low ionic strength (50 mM KCl), the mutated enzyme is characterized by higher cleavage efficiency and by lower religation efficiency when compared to the wild-type enzyme (data not shown). In line, a recent work has shown that the yeast topoisomerase I mutant Thr722Ala (corresponding to the Thr718Ala in the human enzyme) displays a decreased religation rate compared to the wild-type protein, when measured at 50 mM KCl on a 36 oligonucleotide DNA substrate (18).

Root mean square deviations and fluctuations

The experiments described above indicate that upon the single Thr718Ala mutation, the chemistry of the enzyme is unaltered and the relaxation efficiency is reduced. This suggests that the main effect caused by the mutation as detected by experiments carried out at 150 mM KCl ionic strength is a perturbation in the dynamical behavior that alters the control of the DNA

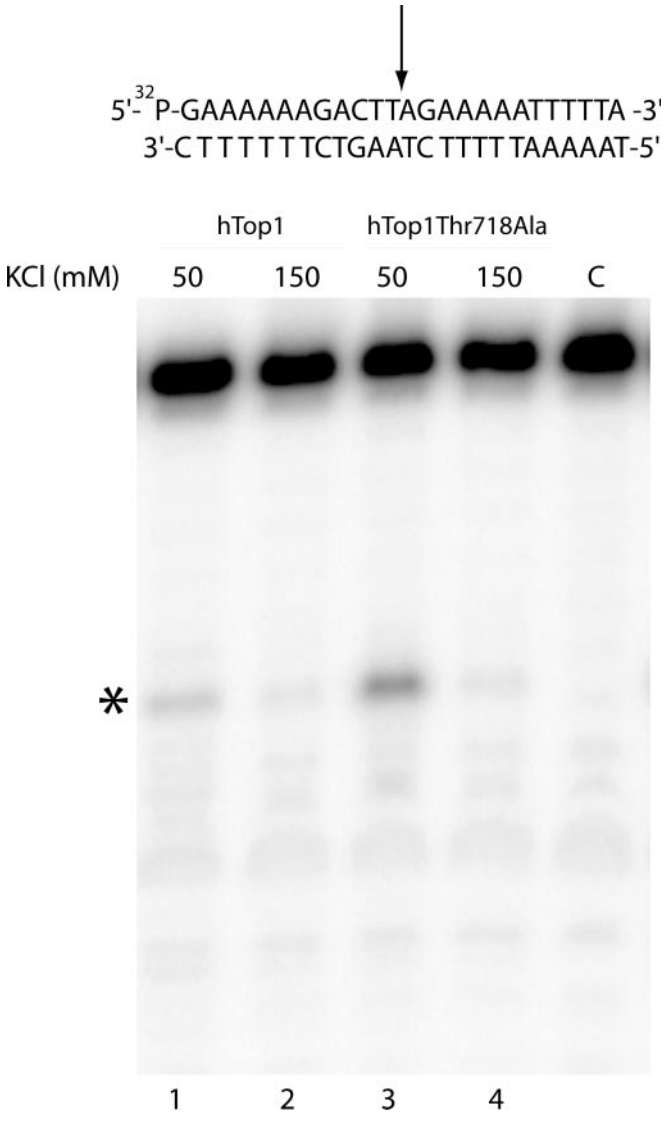

Figure 4. Cleavage/religation equilibrium of DNA oligonucleotide substrate. Lanes 1 and 2 refer to hTop1 protein incubated at 50 and 150 mM KCl respectively with the [γ-^{32}P] end-labeled duplex DNA shown at the top of the figure, where the arrow indicates the preferential cleavage site. Lanes 3 and 4 show the same incubation with hTop1Thr718Ala. The asterisk indicates the band corresponding to the preferential cleavage site. Lane C, no protein added.

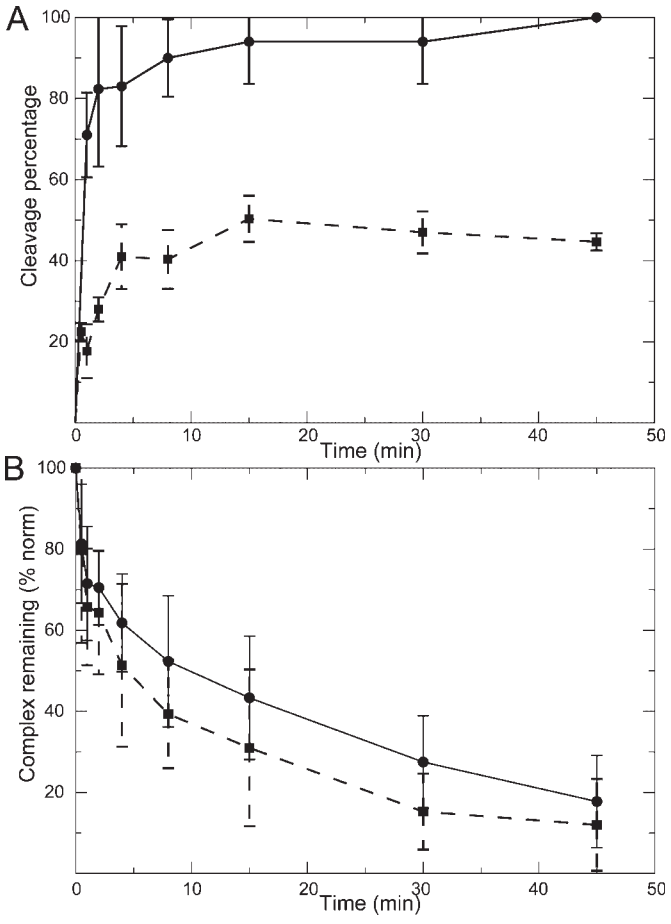

Figure 5. (**A**) Kinetics of cleavage determined by the percentage of the cleaved DNA fragment plotted against time for the hTop1 (filled circles) and hTop1Thr718Ala (filled squares). All values are the average of three different experiments normalized to the plateau of the wild-type enzyme. (**B**) Kinetics of religation determined by the percentage of the remaining covalent complex plotted against time for the hTop1 (filled circles) and hTop1Thr718Ala (filled squares). All values are the average of three different experiments, upon normalization at $t = 0$.

strand rotation. In order to sample the dynamical properties of the mutated enzyme, to be correlated with the above reported experimental findings, we have carried out a 3250 ps long MD simulation of the mutated system, and compared it with an identical simulation carried out on the native enzyme (30).

The RMSD of the native and mutated proteins calculated as a function of simulated time after a mass-weighted superposition on the starting structure is reported in Figure 6A, in black and red colors respectively. The data show that the RMSD of the whole proteins (full lines) oscillates strongly with deviation peaks >3 Å. Upon elimination of the linker domain in the analysis, the RMSD of the core and C-terminal domains (dotted lines) reach a plateau at ∼2 Å after ∼250 ps for both enzymes, and remains constant around this value for the whole simulation time. This result indicates that in both enzymes the linker is the most flexible domain, although to a larger extent for the native protein as will be confirmed in the following sections, and that the systems are well stabilized after 250 ps. Therefore, all the following analyses refer to the last 3000 ps of the trajectory (i.e. from 250 to 3250 ps).

The RMSF of the two simulated systems are represented in Figure 6B, as a function of residue number. The Thr718Ala mutant shows a reduction of fluctuations in residues 674–691 of the linker (i.e. the loop connecting helices 18 and 19, and the entire helix 19) and an increase in the whole core subdomain II. The data indicate that the main differences do not occur in proximity of the mutation, where actually the fluctuations of the native and mutated enzymes are almost identical, but that the Thr718Ala mutant induces dynamical changes in regions contacting the DNA scissile strand.

Principal component analysis

In order to highlight the changes in protein–protein communications induced by the mutation, the principal component

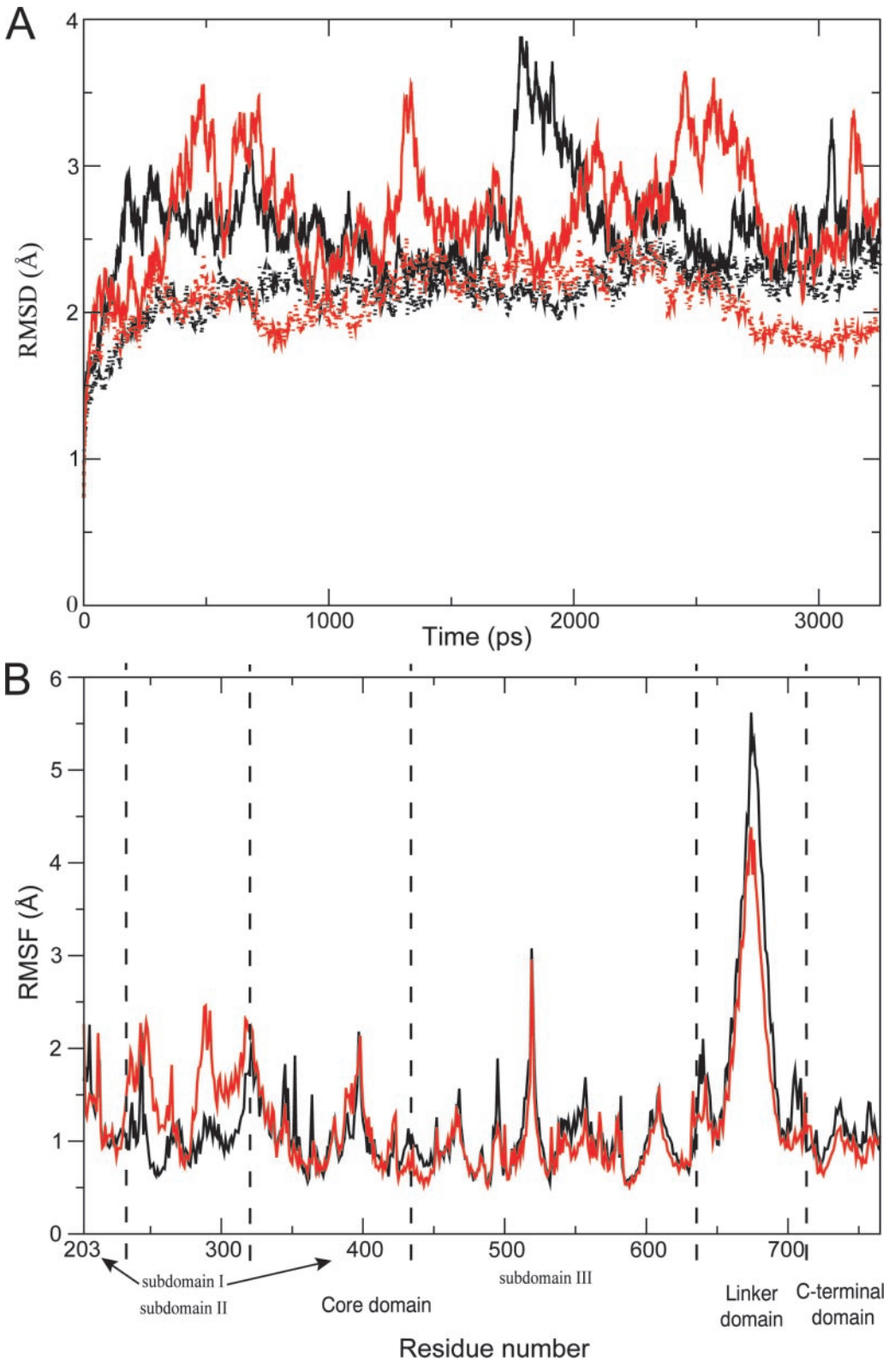

Figure 6. Root mean square deviations (RMSD) and fluctuations (RMSF). (**A**) Protein RMSD from the starting structure are represented as a function of simulation time in black and red full lines for the wild-type and Thr718Ala mutant, respectively. The core and C-terminal domain RMSD are represented in black and red dotted lines for the wild-type and Thr718Ala mutant, respectively. (**B**) The per residue RMSF are represented as a function of the residue number in black and red lines for the wild-type and Thr718Ala mutant, respectively.

analysis has been applied to both the mutated and the native enzyme trajectories to identify the main 3N directions along which the majority of the protein motion is defined (26,27). This analysis is based on the diagonalization of the covariance matrix built from the atomic fluctuations after the removal of the translational and rotational movement, and it has been carried out on the 563 Cα atoms of the protein. The displacement of each Cα along the first eigenvector having the largest eigenvalue shown in Figure 7A, indicates that the linker domain is the protein region with the maximum displacement along this direction for both systems, but with an absolute value larger for the wild-type than for the mutated enzyme. The larger linker fluctuations in the wild-type can be better appreciated looking at the projections of the MD

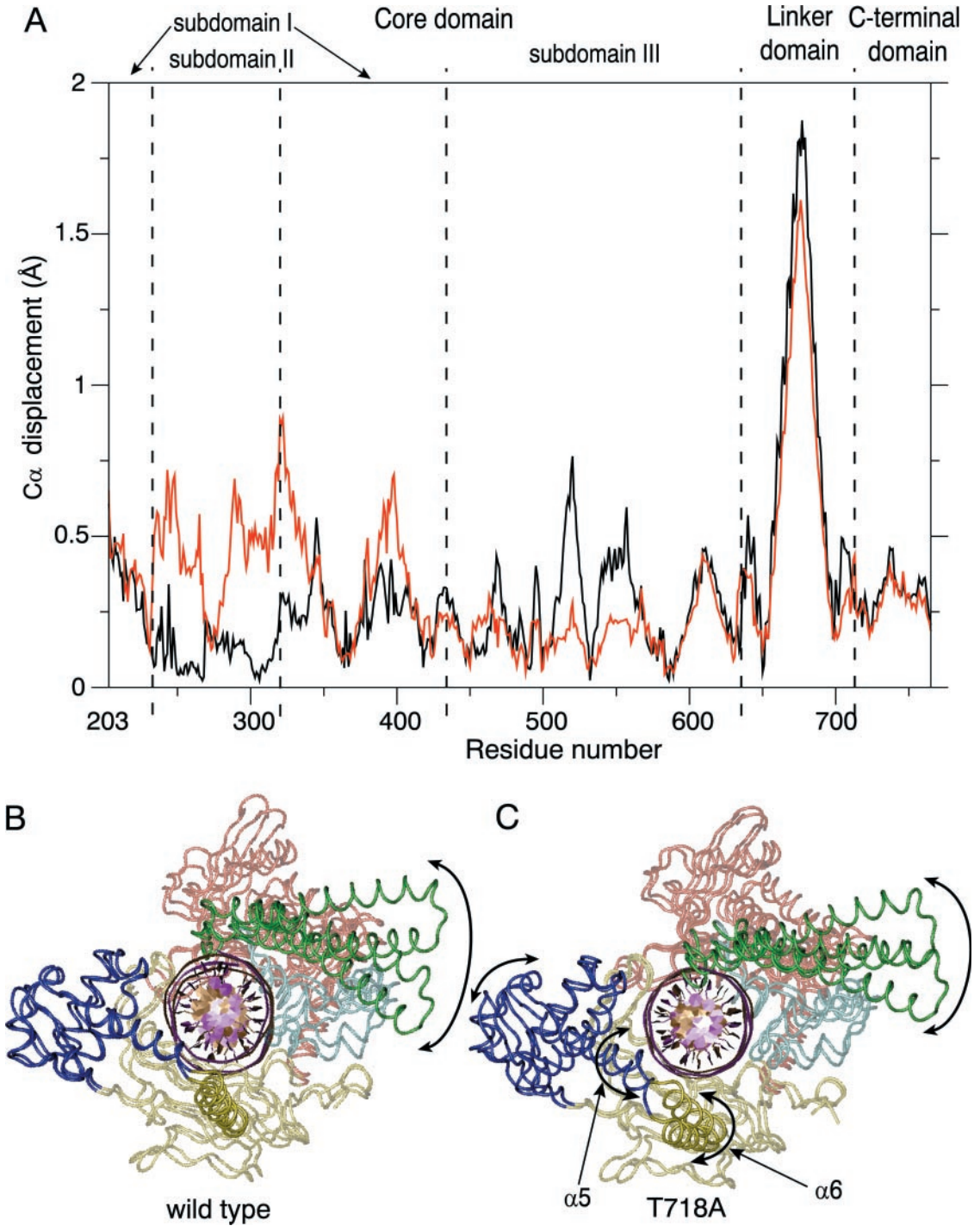

Figure 7. (**A**) Displacements of each Cα atom along the eigenvector with the largest eigenvalue (first eigenvector) are represented in black and red lines for the wild-type and Thr718Ala mutant, respectively. Representation of two extreme projections of the MD motions along the first eigenvector for the wild-type protein (**B**) and mutant proteins (**C**). Black arrows indicate the amplitude and the direction of the motion.

motions along the first eigenvector for the wild-type and mutant proteins shown in Figure 7B and C, respectively. Note that the projections of the protein motions have been represented together with the average protein–DNA structures calculated from the fully unconstrained simulations. Figure 7 also shows an increase in the mutant Cα displacement in the whole core subdomain II and the N-terminal portion of core subdomain I (Figure 7A). The two extreme projections of the MD motions along the first eigenvector illustrate how the motions of the V-shaped α6 from core subdomain I and α5 from core subdomain II are strongly increased upon the Thr718Ala mutation (Figure 7B and C). The principal component analysis indicates that the regions more altered in their dynamics as a result of the single mutation are those contacting the DNA scissile strand, which probably play a role during the DNA relaxation process. A dynamic visualization of the MD projections along the first three eigenvectors are available at NAR Online.

Hydrogen bonds in the mutation site region

As a final analysis, we have calculated the network of the protein–DNA and protein–protein hydrogen bonds, in the proximity of the mutation site. A MD conformation of the Thr718Ala mutant in the proximity of the mutation site, representing the hydrogen bond network formed by the enzyme during the simulation, is shown in Figure 8. The picture shows the involvement of Ala-718 in direct and water-mediated hydrogen bonds with the protein and DNA, respectively.

A hydrogen bond between the side chain of Thr-718 and the G+2 phosphate group of the scissile strand has been detected in several crystallographic structures of topo70 (PDB id 1a36, 1k4s, 1k4t) (6–8). This bond has been proposed to play an important role in the orientation of the +1 5′-OH group during the nucleophilic attack in the religation step (8). The topo70–DNA complex simulation confirms the importance of the Thr-718–G+2 bond, being present during the whole simulation time (data not shown). This hydrogen bond is obviously absent in the Thr718Ala mutant because of the lack of the threonine side chain and analysis of the trajectory indicates that the backbone of alanine forms a direct hydrogen bond with the G+2 phosphate group for only 3% of the simulation time. However, the absence of a direct bond between the Ala-718 and the G+2 base is compensated by a highly stable water-mediated hydrogen bond, present for 95% of the simulation time (Figure 8). In the wild-type enzyme, a similar bond is lacking and a water-mediated hydrogen bond between the side chain of Thr-718 and the G+2 base is present only for 18% of the simulation time.

Deletion of the side chain of Thr-718 also induces changes in the local network of protein–protein hydrogen bonds. In the wild-type enzyme, Thr-718 forms direct hydrogen bonds through its side chain with His-632 and Ser-517, for 43 and 41% of the simulation time respectively, and through its backbone with Leu-721 and Asn-722, for 19 and 23% of the simulation time, respectively (data not shown). In the mutated enzyme, the backbone of Ala-718 forms direct hydrogen bonds with Leu-721 and Asn-722, for 66 and 99% of the simulation time respectively, and with the catalytic Tyr-723 for 18% of the simulation time.

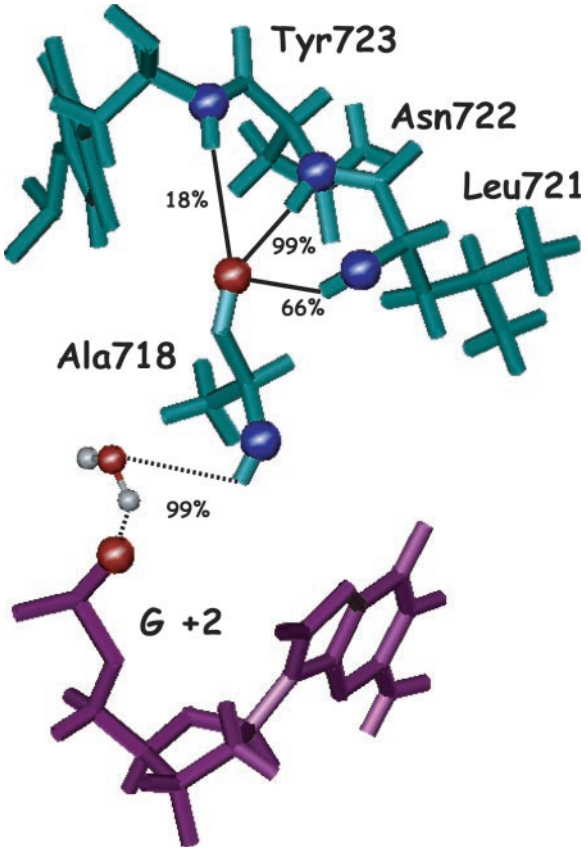

Figure 8. Percentage of hydrogen bonds in the mutation site region evaluated from the MD trajectory. Protein residues and bases are highlighted in cyan and purple, respectively. The oxygen and nitrogen atoms involved in the hydrogen bonds are highlighted with red and blue spheres, respectively. Direct and water-mediated hydrogen bonds are represented in black full and dotted lines, respectively, together with the percentage of their lifetime in the simulation trajectory.

CONCLUSIONS

The results presented here show that at 150 mM KCl the Thr718Ala mutant has a DNA relaxation rate lower than the wild-type enzyme (Figure 3) even though the cleavage/religation equilibrium (Figure 4), the religation rate (Figure 5B) and then the cleavage rate (Figure 5A) are comparable to those of the wild-type enzyme when using as substrate a short linear oligonucleotide containing the preferred cleavage site. A direct comparison between the relaxation rate (Figure 3) and the cleavage and religation rates (Figure 5) is made impossible by the requirement of different substrates in the two sets of experiment, i.e. a supercoiled DNA substrate made by thousands of base pairs in the relaxation experiment and a DNA linear substrate containing 25 bp in the cleavage and religation experiments. On the other hand, the cleavage and religation experiments (Figure 5) can be more directly compared with the equilibrium experiment (Figure 4) since a linear substrate is used in both cases. At physiological ionic strength, the wild-type and mutated enzyme have an identical equilibrium (Figure 4), as well as an identical religation rate (Figure 5B) indicating that at this ionic strength, the reduced relaxation rate of the Thr718Ala mutant is not due to a decreased religation rate but to a lower DNA binding

or to a decreased strand rotation efficiency. The relaxation experiments reported in Figure 3 show a decreased relaxation efficiency of the mutant when compared to the wild-type, independent of the DNA/enzyme ratio. This result excludes that the difference in DNA relaxation between the two proteins can be ascribed to the enzyme substrate association/dissociation rate, implying that the main effect of the single Thr718Ala mutation is associated to the rotation step of the catalysis (29). The *in vitro* biochemical results then provide unambiguous evidences that at physiological ionic strength, the main functional difference between the native and the Thr718Ala mutated Top1 is confined to their strand rotation that is lower for the mutated enzyme.

The MD simulation furnishes an explanation for such an experimental behavior providing structural/dynamical data that permit to interpret the identical religation rate and the difference in the strand rotation. The identical religation rate of the wild-type and the mutated enzyme is actually an unexpected result since it has been suggested that Thr-718 plays a role in the right positioning of the 5′ end through a hydrogen bond between the aminoacidic hydroxyl group and the G+2 phosphate group of the scissile strand (8). The MD trajectory confirms the importance of this hydrogen bond since it is present in the native enzyme for the entire duration of the simulation (30). However, the simulation also shows that upon mutation of the threonine in alanine the lack of the direct hydrogen bond with the G+2 phosphate group is compensated by a water-mediated hydrogen bond to the backbone of Ala-718 (Figure 8). The lack of a similar bond in the wild-type trajectory suggests either that in the mutant, the water-mediated bond plays a main role in the right positioning of the 5′ end, or that Thr-718 does not play any role in the religation rate.

The MD simulation also permits to explain how the mutation of a residue such as Thr-718, which is relatively close to the catalytic site, may have a large effect on the strand rotation step of the catalysis. The plot of the RMSF in fact, indicates that in proximity of the mutation site the two enzymes have identical fluctuations, and that the main differences are localized in the linker domain and in core subdomain II that are supposed to be involved in the DNA strand rotation (6) (Figure 6B). The principal component analysis confirms the RMSF results, showing that, in the mutant, the linker domain and the V-shaped helices are the regions with the major displacement along the first eigenvector (Figure 7).

DNA strand rotation is actually strongly dependent on the enzyme conformation and dynamics. It has been reported that the clamp of the enzyme around DNA crosslinking residue His-367 and Ala-499 still permits strand rotation, but this is no longer possible when the crosslink is made between Gly-365 and Ser-534 (31,32). The fundamental role of the linker domain in modulating the strand rotation has been demonstrated by Champoux and co-workers (9), showing that this domain is required for an efficient CPT inhibition. The increased mobility of the linker has been shown to be the most likely explanation for the CPT resistance displayed by the mutant in which alanine at 653 is substituted with a proline (10). Multiple mutations in the linker domain render the enzyme hypersensitive to the drug, indicating the occurrence of protein communications between this domain and the drug binding pocket (33). Finally, a direct correlation between inhibitor and linker mobility has been shown upon a comparison of the electron density maps of the enzyme crystals in the presence or absence of Topotecan (8).

Here, we show the existence of a direct communication between two regions located far away, i.e. the region close to the active site and the linker domain. In fact, the Thr718Ala mutation induces different flexibility in the linker and in the V-shaped α helices (Figures 6B and 7), confirming the interesting correlation between linker mobility and DNA relaxation efficiency. Moreover, the experimental data show that strand rotation is an important step in the catalytic process and that is directly controlled by the enzyme. In line, a recent report measuring real-time single-molecule DNA relaxation has shown that Top1 releases DNA supercoils by a swivel mechanism that involves friction between the rotating DNA and the enzyme, underlining the importance of the enzyme dynamic properties (34).

Taken together, these results indicate that for topoisomerase I the description of the structural/dynamical properties are an important achievement to fully understand its function and must be taken into account for the design of new drugs with improved efficiency.

SUPPLEMENTARY MATERIAL

Supplementary Material is available at NAR Online.

ACKNOWLEDGEMENTS

We thank Mary-Ann Bjornsti for helpful discussion during the preparation of the manuscript and S.Z. Pedersen for his careful review of this article. This work was partly supported by grants from MURST COFIN2003, from Ministero della Salute, from FIRB project on Bioinformatics for Genomics and Proteomics and FIRB project for Functional Genomics. Funding to pay the Open Access publication charges for this article was provided by MURST COFIN2003.

Conflict of interest statement. None declared.

REFERENCES

1. Chen,A. and Liu,L.F. (1994) DNA topoisomerases: essential enzymes and lethal targets. *Annu. Rev. Pharmacol. Toxicol.*, **34**, 191–218.
2. Nitiss,J. (1998) Investigating the biological functions of DNA topoisomerases in eukaryotic cells. *Biochim. Biophys. Acta*, **1400**, 63–82.
3. Wang,J.C. (1996) DNA topoisomerases. *Annu. Rev. Biochem.*, **65**, 635–692.
4. Stewart,L., Ireton,G.C. and Champoux,J.J. (1996) The domain organization of human topoisomerase I. *J. Biol. Chem.*, **271**, 7602–7608.
5. Redinbo,M.R., Stewart,L., Kuhn,P., Champoux,J.J. and Hol,W.G.J. (1998) Crystal structures of human topoisomerase I in covalent and noncovalent complexes with DNA. *Science*, **279**, 1504–1513.
6. Stewart,L., Redinbo,M.R., Qiu,X., Hol,W.G.J. and Champoux,J.J. (1998) A model for the mechanism of human topoisomerase I. *Science*, **279**, 1534–1541.
7. Pommier,Y., Pourquier,P., Fan,Y. and Strumberg,D. (1998) Mechanism of action of eukaryotic DNA topoisomerase I and drugs targeted to the enzyme. *Biochim. Biophys. Acta*, **1400**, 83–105.
8. Staker,B.L., Hjerrild,K., Feese,M.D., Behnke,C.A., Burgin,A.B.,Jr and Stewart,L. (2002) The mechanism of topoisomerase I poisoning by a camptothecin analog. *Proc. Natl Acad. Sci. USA*, **99**, 15387–15392.

9. Stewart,L., Ireton,G.C. and Champoux,J.J. (1999) A functional linker in human topoisomerase I is required for maximum sensitivity to camptothecin in a DNA relaxation assay. *J. Biol. Chem.*, **274**, 32950–32960.
10. Fiorani,P., Bruselles,A., Falconi,M., Chillemi,G., Desideri,A. and Benedetti,P. (2003) Single mutation in the linker domain confers protein flexibility and camptothecin resistance to human topoisomerase I. *J. Biol. Chem.*, **278**, 43268–43275.
11. Champoux,J.J. (2000) Structure-based analysis of the effects of camptothecin on the activities of human topoisomerase I. *Ann. N. Y. Acad. Sci.*, **922**, 56–64.
12. Megonigal,M.D., Fertala,J. and Bjornsti,M.-A. (1997) Alterations in the catalytic activity of yeast DNA topoisomerase I result in cell cycle arrest and cell death. *J. Biol. Chem.*, **272**, 12801–12808.
13. Fiorani,P., Amatruda,J.F., Silvestri,A., Butler,R.H., Bjornsti,M.-A. and Benedetti,P. (1999) Domain interactions affecting human DNA topoisomerase I catalysis and camptothecin sensitivity. *Mol. Pharmacol.*, **56**, 1105–1115.
14. Bjornsti,M.-A., Benedetti,P., Viglianti,G.A. and Wang,J.C. (1989) Expression of human DNA topoisomerase I in yeast cells lacking yeast DNA topoisomerase I: restoration of sensitivity of the cells to the antitumor drug camptothecin. *Cancer Res.*, **49**, 6318–6323.
15. Kauh,E.A. and Bjornsti,M.-A. (1995) SCT1 mutants suppress the camptothecin sensitivity of yeast cells expressing wild-type DNA topoisomerase I. *Proc. Natl Acad. Sci. USA*, **92**, 6299–6303.
16. Bjornsti,M.-A. and Wang,J.C. (1987) Expression of yeast DNA topoisomerase I can complement a conditional-lethal DNA topoisomerase I mutation in *Esherichia coli*. *Proc. Natl Acad. Sci. USA*, **84**, 8971–8975.
17. Benedetti,P., Fiorani,P., Capuani,L. and Wang,J.C. (1993) Camptothecin resistance from a single mutation changing glycine 363 of human DNA topoisomerase I to cysteine. *Cancer Res.*, **53**, 4343–4348.
18. Colley,W.C., Van Der Merwe,M., Vance,J.R., Burgin,A.B.,Jr and Bjornsti,M.-A. (2004) Substitution of conserved residues within the active site alters the cleavage religation equilibrium of DNA topoisomerase I. *J. Biol. Chem.*, **279**, 54069–54078.
19. Yang,Z. and Champoux,J.J. (2002) Reconstitution of enzymatic activity by the association of the cap and catalytic domains of human topoisomerase I. *J. Biol. Chem.*, **277**, 30815–30823.
20. Cornell,W.D., Cieplak,P., Bayly,C.I., Gould,I.R., Kenneth,M., Merz,J., Ferguson,D.M., Spellmeyer,D.C., Fox,T., Caldwell,J.W. and Kolman,P.A. (1995) A second generation force field for the simulation of proteins, nucleic acids, and organic molecules. *J. Am. Chem. Soc.*, **117**, 5179–5197.
21. Jorgensen,W.L., Chandrasekhar,J., Madura,J.D., Impey,R.W. and Klein,M.L. (1983) Comparison of simple potential functions for simulating liquid water. *J. Chem. Phys.*, **79**, 926–935.
22. Darden,T., York,D. and Pedersen,L. (1993) Particle mesh Ewald: an N.log(N) method for Ewald sums in large systems. *J. Chem. Phys.*, **98**, 10089–10092.
23. Cheatham,T.E., Miller,J.L., Fox,T., Darden,T.A. and Kollman,P.A. (1995) Molecular dynamics simulation on solvated biomolecular systems: the particle mesh Ewald method leads to stable trajectories of DNA, RNA, and proteins. *J. Am. Chem. Soc.*, **117**, 4193–4194.
24. Ryckaert,J.-P., Ciccotti,G. and Berendsen,H.J.C. (1977) Numerical integration of the Cartesian equations of motion of a system with constraints: molecular dynamics of n-alkanes. *J. Comput. Phys.*, **23**, 327–341.
25. Berendsen,H.J.C., Postma,J.P.M., van Gusteren,W.F., Di Nola,A. and Haak,J.R. (1984) Molecular dynamics with coupling to an external bath. *J. Comput. Phys.*, **81**, 3684–3690.
26. Garcia,A.E. (1992) Large-amplitude nonlinear motions in proteins. *Phys. Rev. Lett.*, **68**, 2696–2699.
27. Amadei,A., Linssen,A.B. and Berendsen,H.J. (1993) Essential dynamics of proteins. *Proteins*, **17**, 412–425.
28. Berendsen,H.J.C., van der Spoel,D. and van Drunen,R. (1995) GROMACS: a message-passing parallel molecular dynamics implementation. *Comp. Phys. Commun.*, **95**, 43–56.
29. Frohlich,R.F., Andersen,F.F., Westergaard,O., Andersen,A.H. and Knudsen,B.R. (2004) Regions within the N-terminal domain of human topoisomerase I exert important functions during strand rotation and DNA binding. *J. Mol. Biol.*, **336**, 93–103.
30. Chillemi,G., Redinbo,M., Bruselles,A. and Desideri,A. (2004) Role of the linker domain and the 203–214 N-terminal residues in the human topoisomerase I DNA complex dynamics. *Biophys J.*, **87**, 4087–4097.
31. Woo,M.H., Losasso,C., Guo,H., Pattarello,L., Benedetti,P. and Bjornsti,M.-A. (2003) Locking the DNA topoisomerase I protein clamp inhibits DNA rotation and induces cell lethality. *Proc. Natl Acad. Sci. USA*, **100**, 13767–13772.
32. Carey,J.F., Schultx,S.J., Sisson,L., Fazzio,T.G. and Champoux,J.J. (2003) DNA relaxation by human topoisomerase I occurs in the closed clamp conformation of the protein. *Proc. Natl Acad. Sci. USA*, **100**, 5640–5645.
33. Scaldaferro,S., Tinelli,S., Borgnetto,M.E., Azzini,A. and Capranico,G. (2001) Directed evolution to increase camptothecin sensitivity of human DNA topoisomerase I. *Chem. Biol.*, **8**, 871–881.
34. Koster,D.A., Croquette,V., Dekker,C., Shuman,S. and Dekker,N.H. (2005) Friction and torque govern the relaxation of DNA supercoils by eukaryotic topoisomerase IB. *Nature*, **434**, 671–674.